Switch Opening and Exchange Method for Stochastic Distribution Network Reconfiguration

Junpeng Zhan, *Member, IEEE,* Weijia Liu, *Member, IEEE*, C. Y. Chung, *Fellow, IEEE*, and Jiajia Yang, *Member, IEEE*

***Abstract*—The purpose of distribution network reconfiguration (DNR) is to determine the optimal topology of an electricity distribution network, which is an efficient measure to reduce network power losses. Electricity load demand and photovoltaic (PV) output are uncertain and vary with time of day, and will affect the optimal network topology. Single-hour deterministic DNR is incapable of handling this uncertainty and variability. Therefore, this paper proposes to solve a multi-hour stochastic DNR (SDNR). Existing solution methods for DNR are either inaccurate or excessively time-consuming, and are therefore incapable of solving multi-hour SDNRs for large distribution networks. In this regard, a switch opening and exchange (SOE) method is proposed. Starting from a looped network with all switches closed, the SOE consists of three steps. The first step is to sequentially open the switches until all of the loops are opened. The second and third steps modify the status of branches obtained in the first step to obtain better radial topologies. Five test systems are used to validate the accuracy and fast solution speed of the SOE and the superiority of multi-hour SDNR over single-hour deterministic DNR.**

***Index Terms*—Distribution network reconfiguration (DNR); multi-hour stochastic DNR; photovoltaics (PV); radiality.**

NOMENCLATURE

Superscript/subscript

D, G	Demand and generation, respectively
t, s	Time and scenario, respectively
ij	Branch index (connecting nodes i and j)
i	Bus index

Parameter/variable

B_{ij}, G_{ij}	Imaginary and real parts of the ith row and jth column of the admittance matrix, respectively
L_x	Vectors of losses, x =1,2,3
n_b	Number of buses
n_l	Number of branches
PF	Power factor
p_s^t	Probability of scenario s
$P_{i,s}^{t,D}$	Active power demand at bus i
$P_{i,s}^{t,G}$	Total active power generation at bus i
$P_{i,s}^{t,G,conv}$	Active power generated by conventional generators at bus i
$P_{i,s}^{t,G,PV}$	Active power generated by photovoltaic (PV) at bus i
$Q_{i,s}^{t,D}$	Reactive power demand at bus i
$Q_{i,s}^{t,G}$	Total reactive power generation at bus i
$Q_{i,s}^{t,G,conv}$	Reactive power generated by conventional generators at bus i
$Q_{i,s}^{t,G,PV}$	Reactive power generated by PV at bus i
R_{ij}, X_{ij}	Resistance and reactance on branch i-j, respectively
T	Total periods of time considered
$\bar{S}_{ij}$	Maximum allowable apparent power on branch i-j
S_e, S_s	Two sets containing sectionalizing switches used in Algorithms 3 and 2, respectively
$V_{i,s}^t$ ($V_{j,s}^t$)	Voltage magnitude at bus i (j)
V_i^{min}	Minimum voltage magnitude allowed at bus i
V_i^{max}	Maximum voltage magnitude allowed at bus i
β_{ij} (β_l)	Binary variable used to indicate open/closed status of switch i-j (l): 1 represents closed and 0 represents open
Δt	Time interval (1 hour)
$\delta_{i,s}^t$	Voltage angle at bus i
Ω_B, Ω_S	Sets of all branches and all scenarios, respectively
Ω_i	A set of nodes having branches connected to node i

The work was supported in part by the Natural Sciences and Engineering Research Council (NSERC) of Canada and the Saskatchewan Power Corporation (SaskPower).

Junpeng Zhan is with the Sustainable Energy Technologies Department, Brookhaven National Laboratory, Upton, NY 11973, U.S.A. (e-mail: jzhan@bnl.gov).

Weijia Liu is with Power System Engineering Center, National Renewable Energy Laboratory (NREL), Golden, CO 80401, U.S.A. (e-mail: weijia.liu@nrel.gov).

C. Y. Chung is with the Department of Electrical and Computer Engineering, University of Saskatchewan, Saskatoon, SK S7N 5A9, Canada (e-mail: c.y.chung@usask.ca).

Jiajia Yang is with the School of Electrical Engineering and Telecommunications, University of New South Wales, Sydney, NSW 2052, Australia (e-mail: jiajia.yang@unsw.edu.au).

I. INTRODUCTION

ELECTRICITY distribution systems have recently received increasing attention. A distribution network usually operates in a radial topology [1], i.e., each node has exactly one path to the substation node and the network has no loops. Switches in a distribution network can be divided into two types: tie switches that are normally open and sectionalizing switches that are normally closed [2]. Distribution network reconfiguration (DNR) aims to optimize the network topology by changing the open/closed status of switches, which is one of the most important ways to enhance system performance [3-5], e.g., loss reduction. The objective of DNR is usually to minimize power losses, although some researchers use other objectives such as enhancing reliability and improving power quality [6].

Photovoltaics (PV) power is an important clean energy source experiencing fast growth. According to the International Energy Agency, PV is expected to provide 5% (11%) of global electricity production by 2030 (2050) [7]. PV output varies with time of day: it usually reaches a maximum from 12:00 to 14:00 and is zero at night. PV output is also uncertain, i.e., is very difficult to predict with high accuracy.

As more distributed generations (DGs) are being used in distributed systems, using DNR to manage the distribution systems becomes more important. Recently, researchers have investigated the DNR for unbalanced distribution system [3][8], outage management [9], annual energy loss reduction [10], state estimation [11], ADS with EV [12], ADS with DG and prosumer controllable loads [13], etc. Another type of research about DNR focuses on improving computational efficiency and it includes parallel computing on GPU [14], extended fast decoupled power flow [15], Benders decomposition [16][17], and speeding up the calculation of repeated power flow [13].

Many existing research focuses on single-hour DNR [18-20], where the load is set to its peak value. When PV is considered, the topology obtained from single-hour DNR is not optimal for different hours of the day as PV output varies significantly with time. To address this issue, researchers use hourly DNR (also called dynamic DNR) [8][21] or multi-hour DNR [22]. Hourly DNR solves a single-hour DNR for each hour of the day independently [21], with the solutions obtained having a minimum objective, usually in terms of power loss, for each hour. However, the solutions obtained can involve a large number of switching actions (i.e., opening/closing switches). Frequent switching actions can affect system stability [23], increase the work burden of the system operator, and even shorten the lifetime of the switch [24]. In [22], multi-hour DNR is solved by mathematical programming (MP) where the network topology is assumed to be unchanged during each 8-hour period to avoid frequent switching actions. However, multi-hour DNR for a large system has a large number of constraints and variables (both binary and continuous) and is therefore very difficult to solve by using MP.

Both load demand and PV output for the next day are uncertain, i.e., their predicted values have errors. In a deterministic DNR (DDNR) [18-20, 22], the load demand and PV output are assumed to be equal to fixed values. However, the result obtained from the DDNR can have a high power loss [24] or even be infeasible [25] when the load demand and/or PV output deviate from their predicted values. To address this issue, robust optimization [24, 25] and interval optimization [26] for DNR have been studied. Robust/interval optimization can obtain a topology that is feasible when the load demand and PV output vary within a certain range; however, neither consider the high/low probability of different scenarios and therefore can lead to conservative solutions.

Two factors complicate solving a DNR problem, i.e., the non-linearity of AC power flow and the requirement of network radiality. Note that the aim of DNR is to obtain a radial network; this is assumed throughout the literature we have seen [1-2, 18-30] and is also adopted in this paper. To handle the first factor, researchers used DC power flow, a Distflow model [27] that is a second-order MP model, and full AC power flow [20]. However, the DC power flow model is inaccurate while the Distflow and the full AC power flow models are accurate but very time-consuming for a large system. The methods to ensure radiality in the DNR problem can be divided into three types: loop-based [2, 6, 19], path-based [18], and node-based [20, 22, 28]. The first two types are mainly used in evolutionary algorithms (EAs) and are difficult to employ in MP methods. These two types are not discussed in detail because EAs are not the focus of this paper (as discussed in the next paragraph). Node-based methods are mainly used in the MP model for DNR, and can be further divided into two sub-types. The first sub-type is the spanning tree method [22], the main idea of which is that every node except the substation node has exactly one parent node. In the second sub-type [20, 28], radiality is ensured because the number of branches is one less than the number of nodes and each node with load has a path to the substation node (i.e., is not isolated). The method to ensure radiality used in this paper is similar to the second sub-type.

The solution methods for the DNR can be divided into three types, i.e., heuristics [29, 30], EA [2, 6, 18, 19], and MP [20, 22, 23, 27-28] based approaches. Ref. [31] has provided a holistic review of different approaches for DNR. EAs perform well in small systems but might converge slowly, especially in large systems. Moreover, the results obtained by EAs for different runs might not be the same, which prevents them from being widely used in power system applications. In an MP model for DNR, the open/closed status of each branch is represented by a binary variable, which results in a combinatorial explosion in the number of total possible solutions as the number of branches increases. For a system with 136 switches, the number of total possible solutions is $2^{136} = 8.7 \times 10^{40}$, which is a huge number. Therefore, the MP method can be too time-consuming to solve a single-hour DNR problem in a large system, not to mention a large-scale multi-hour stochastic DNR (SDNR) problem.

This paper focuses on heuristic algorithms. Heuristic algorithms mainly employ two types of strategies [31]: sequential switch opening and branch exchanging. Using only one of the two strategies suffers an accuracy problem. To address this issue and to efficiently solve a large-scale multi-hour SDNR problem, this paper proposes a switch opening and exchange (SOE) method, which uses both types of strategies mentioned above. The SOE method consists of three steps where the first step employs the sequential switch opening strategy while the second and third steps are based on the branch exchanging strategy. The initial status of each branch in a distribution network is set to be closed and the network has loops. To achieve a radial network, some of the originally all-closed switches need to be opened, i.e., they are selected as the tie switches. In an MP or EA, different dimensions of a solution are optimized in a simultaneous manner, i.e., the status of all switches can change simultaneously in a single iteration, which is time-consuming when solving the DNR in a large system. In contrast, the first step of the SOE method uses a sequential manner to determine

different dimensions of a solution, i.e., only one switch can change its status in a single iteration.

In each iteration of the first step, one sectionalizing switch is changed to a tie switch, which opens a loop. The iteration stops when all loops have been opened, i.e., a radial network has been obtained. The topology obtained in this step is referred to as the *initial topology*. In the second step, a set of closed switches in the initial topology are chosen and, for each switch in the chosen set, its status is forced to open and the first step will be executed to obtain another topology. In the third step, for each topology obtained in the first two steps, the open/closed statuses of the switches near the ending nodes of the network are changed to obtain different topologies. This is the main idea of the SOE method.

The contributions of this paper include 1) proposing a novel heuristic method, i.e., SOE, which is superior to other heuristic algorithms, EAs, and MPs in terms of accuracy and/or solution speed; this is the main contribution of the paper and 2) verifying, for the first time, that a multi-hour SDNR can obtain a solution with a good trade-off between minimizing energy losses and the number of switching actions and is superior to both single-hour DNR and DDNR. Considering that existing methods are insufficient in solving a multi-hour SDNR, especially for a large system, the SOE advances the frontiers of the solution methods for complicated DNR.

The rest of the paper is organized as follows. The model for multi-hour SDNR is given in Section II. The SOE method is detailed in Section III. Simulation results are given in Section IV. Conclusions are given in Section V.

II. Stochastic Distribution Network Reconfiguration

The multi-hour SDNR model can be represented by (1)-(11):

$$\text{Minimize: } \sum_{t=1}^{T}\sum_{s\in\Omega_s}\sum_{ij\in S_B} p_s^t\beta_{ij}\left(\frac{V_{i,s}^t\angle\delta_{i,s}^t - V_{j,s}^t\angle\delta_{j,s}^t}{R_{ij}+jX_{ij}}\right)^2 R_{ij}\,\Delta t \quad (1)$$

$$\text{s.t. } P_{i,s}^{t,G} - P_{i,s}^{t,D} = \sum_{j\in\Omega_i}\beta_{ij}G_{ij}V_{i,s}^tV_{j,s}^t\cos\delta_{ij,s}^t + \sum_{j\in\Omega_i}\beta_{ij}B_{ij}V_{i,s}^tV_{j,s}^t\sin\delta_{ij,s}^t,\ \forall t,\forall s,\forall i \quad (2)$$

$$Q_{i,s}^{t,G} - Q_{i,s}^{t,D} = \sum_{j\in\Omega_i}\beta_{ij}V_{i,s}^tV_{j,s}^tG_{ij}\sin\delta_{ij,s}^t - \sum_{j\in\Omega_i}\beta_{ij}V_{i,s}^tV_{j,s}^tB_{ij}\cos\delta_{ij,s}^t,\ \forall t,\forall s,\ \forall i \quad (3)$$

$$\beta_{ij}\left(V_{i,s}^tV_{j,s}^t\right)^2[(G_{ij}\cos\delta_{ij,s}^t + B_{ij}\sin\delta_{ij,s}^t)^2 + (G_{ij}\sin\delta_{ij,s}^t - B_{ij}\cos\delta_{ij,s}^t)^2] \le \beta_{ij}\bar{S}_{ij}^2,\ \forall t,\forall s,\forall ij\in\Omega_B \quad (4)$$

$$V_i^{min} \le V_{i,s}^t \le V_i^{max},\ \forall t,\forall s,\forall i \quad (5)$$

$$P_{i,s}^{t,G} = P_{i,s}^{t,G,conv} + P_{i,s}^{t,G,PV},\ \forall t,\forall s,\forall i \quad (6)$$

$$Q_{i,s}^{t,G} = Q_{i,s}^{t,G,conv} + Q_{i,s}^{t,G,PV},\ \forall t,\forall s,\forall i \quad (7)$$

$$\sum_{s\in\Omega_s} p_s = 1 \quad (8)$$

where $\delta_{ij,s}^t = \delta_{i,s}^t - \delta_{j,s}^t$. The objective function, (1), minimizes the energy loss. Note that minimizing energy loss is equivalent to minimizing power loss in (1) as the only difference between them is whether Δt exists. This paper minimizes energy loss instead of power loss because the losses in different hours need to be added together. In the rest of the paper, the 'loss' refers to energy loss. Eqs. (2) and (3) represent active and reactive power balance, respectively. Eq. (4) represents the maximum capacity limit of branch i-j. Eq. (5) represents the upper and lower bounds of voltage for each bus. Eqs. (6) and (7) reflect that the nodal active and reactive power generation consist of conventional generators and PV, respectively. In (1), T is the total number of periods and each period is assumed to be one hour in this paper. Eq. (8) guarantees that the sum of the probabilities of all scenarios is equal to one.

A. Handling the PV

The PV output can be represented as a fixed power factor model [32, 33] as shown in (9). The node with PV can then be treated as a PQ bus in the power flow calculation. The uncertainty of PV output is captured as scenarios. This is a high-level model without detailed modeling of PV output and, therefore, is also suitable for modeling wind power output.

$$P_{i,s}^{t,G,PV}\Big/\sqrt{\left(P_{i,s}^{t,G,PV}\right)^2 + \left(Q_{i,s}^{t,G,PV}\right)^2} = \text{PF},\ \ \forall s,\forall i \quad (9)$$

B. Radiality and Connectivity

$$n_b - n_l = 1 \quad (10)$$

$$d(i, i_{\text{substation}}) < \infty,\ \forall i \ne i_{\text{substation}} \quad (11)$$

Eq. (10) represents the relationship between the number of buses and the number of closed branches, which is the necessary condition of a radial network based on graph theory. In (11), $d(i, i_{\text{substation}})$ represents the distance between node i and the substation node, which is finite when a path between them exists. Eq. (11) indicates that the network is connected and has no isolated nodes. Eqs. (10) and (11) should be satisfied in each scenario and guarantee the radiality and connectivity of a network.

Model (1)-(11) is a single-hour (multi-hour) SDNR when T=1 (T>1). If Ω_s has only one element and $p_s^t = 1$, model (1)-(11) degrades to a DDNR.

III. Switch Opening and Exchange Method

The SOE method consists of three steps that are detailed in the following three subsections, respectively. Before executing SOE, the status of each switch is set to closed and the network has loops.

A. Step 1: Sequentially Switch Opening

The number of iterations in step 1 is equal to the number of loops in the original all-switch-closed network. One switch is selected and opened in each iteration, i.e., one tie switch is selected. This switch must be within a loop so that opening this switch opens a loop but does not isolate any buses. Furthermore, opening this switch results in a smaller loss increase than opening any other single switch within any loop. This is a sequential way to determine the tie switches of a distribution system. The detailed procedure of step 1 is given as follows:

- Step 1.1: Obtain the generation, load, and topology information of a system and find all the switches in loops.

- Step 1.2: Open a switch in a loop and check the connectivity of the system via (11). If each node has a path to the substation, solve (1)-(9) and save the loss value in a vector, L_1; otherwise, assign a large positive number to the objective value and store it in L_1. Close the switch opened in this step. Note that constraints (2)-(9) need to be satisfied in each scenario and if any constraint is not satisfied, a large positive number will be assigned as the objective value and stored in L_1.
- Step 1.3: Repeat step 1.2 until all of the switches in loops have been traversed.
- Step 1.4: Find the minimum objective obtained in steps 1.2 and 1.3 from L_1 and open the switch associated with this minimal objective.
- Step 1.5: Repeat steps 1.2-1.4 until (10) is satisfied, i.e., the system is radial.

Note that the topology obtained in step 1 will be used as an input to both steps 2 and 3. The pseudo code of step 1 is provided in Algorithm 1.

Algorithm 1: Pseudo code of step 1

Obtain the generation, load, and topology information of a system and find all the switches in loops. (*step 1.1*)
stop_flag=0.
while stop_flag=0 **do** (*step 1.5*)
  for each switch l in loops **do** (*steps 1.2-1.3*)
    Open switch l, i.e., $\beta_l = 0$.
    if each node is connected to the substation (i.e., (11) is satisfied) **then**
      Solve (1)-(9) and assign the objective calculated via (1) to $L_1(l)$. If any constraints in (2)-(9) are not satisfied, let $L_1(l)=1 \times 10^6$.
    else
      $L_1(l)=1 \times 10^6$.
    end if
    Close switch l, i.e., $\beta_l = 1$.
  end for
  Find the minimum value in L_1 and let k be the value of l for which $L_1(l)$ attains its minimum, i.e., $k = \arg\min_l L_1(l)$. Open switch k, i.e., $\beta_k = 0$. (*step 1.4*)
  if the system is radial (i.e., (10) is satisfied) **then**
    stop_flag=1.
  end if
end while

Solving model (1)-(9) for a fixed network topology in step 1.2 is equivalent to solving an AC power flow for each scenario of each hour, which is not time-consuming. As will be shown in the simulation section below, step 1 can obtain an accurate solution for a small system. However, the solution obtained in step 1 is not close to the optimal solution (the relative error between them might be as high as 5%). As mentioned in Section I, the topology obtained in step 1 is referred to as the initial topology. The method given in [30] is similar to step 1 but faster and faces the same problem of inaccuracy as step 1. Note that neither PV nor uncertainty is considered in [30]. To obtain a more accurate solution based on the solution obtained in step 1, two strategies are proposed to change the initial topology in the following two subsections, respectively.

B. Step 2: Change a Sectionalizing Switch in the Initial Topology to a Tie Switch

For the convenience of expression, two terms are defined in the following.

Upstream and downstream: Upstream and downstream are used only in radial networks in this paper. If and only if node/branch/switch x is in the shortest path from node/branch/switch y to the substation node, the former is upstream of the latter and the latter is downstream of the former. All branches/switches are downstream of the substation node and all nodes except the substation node are downstream of the substation node. For example, in Fig. 1, node 23 is upstream of nodes 24 and 25 and nodes 24 and 25 are downstream of node 23.

Ending node: This refers to a node that has no downstream nodes, e.g., nodes 7, 10, 14, 25, 32, and 33 in Fig. 1.

1) General Description of Step 2

It is assumed that each branch has one and only one switch, either a sectionalizing switch or tie switch. According to (10), the number of sectionalizing switches in a radial system is equal to the number of nodes minus one. The initial topology is represented by a set of sectionalizing switches.

The objective of step 2 is to obtain different topologies from the initial topology expecting that better solutions can be obtained. A straightforward process to achieve this objective is to change a sectionalizing switch to a tie switch (i.e., open a switch that is closed in the initial topology) and execute step 1 to obtain a different topology; note that the status of this switch is forced to open when executing step 1. This process can be repeated for different sectionalizing switches to obtain different topologies. That is, step 2 needs to execute step 1 as many times as the number of sectionalizing switches in the initial topology, which introduces a high computational burden if the number of nodes in a system is large. To alleviate this problem, the above-mentioned process is not repeated for all of the sectionalizing switches, i.e., excluding the following three types of sectionalizing switches in the initial topology. The rationale for excluding these switches is given in Section III-B3.

- Type-1 switch: Any sectionalizing switch whose shortest path to the substation node consists of n_1 or fewer sectionalizing branches in the initial topology.
- Type-2 switch: Any sectionalizing switch in the initial topology satisfying: 1) its shortest path to an ending node consists of n_2 or fewer sectionalizing branches and 2) it is upstream of the same ending node.
- Type-3 switch: Any sectionalizing switch that is not in a loop of the original all-switch-closed network.

Fig. 1 is used to illustrate these three types of switches. In Fig. 1, the solid (dashed) lines represent the branches associated with the sectionalizing (tie) switches. In the following, switch i-j represents the switch associated with branch i-j. The path from switch 1-2 to the substation node has one sectionalizing branch. The path from switch 2-3 (or switch 2-19) to the substation node has two sectionalizing branches. If $n_1 = 3$, then the type-1 switches include 1-2, 2-3, 2-19, 3-23, 3-4, and 19-20.

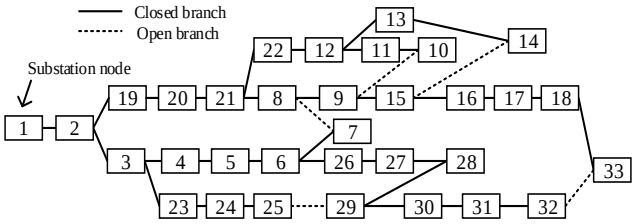

Fig. 1. The 33-node test system.

The shortest path from switch 24-25 (23-24) to ending node 25 has one sectionalizing branch (two sectionalizing branches). If $n_2 = 2$, then the type-2 switches include 24-25, 23-24, 6-7, 5-6, 31-32, 30-31, 18-33, 17-18, 13-14, 12-13, 11-10, and 12-11. Fig. 1 has only one type-3 switch, i.e., switch 1-2.

2) Detailed Procedure of Step 2

The detailed procedure of step 2 is as follows:

- Step 2.1: Let set S_s represent all the sectionalizing switches in the initial topology.
- Step 2.2: Exclude type-1, type-2, and type-3 switches from S_s.
- Step 2.3: Change switch l in S_s to a tie switch (i.e., force the status of switch l to open), close all the other switches, and execute step 1 to obtain a radial topology. Store the obtained topology that is used to calculate the objective via (1). Store the calculated loss.
- Step 2.4: Change switch l back to a sectionalizing switch.
- Step 2.5: Repeat steps 2.3-2.4 for each switch in S_s.

Note that each radial topology obtained in step 2 will be used as an input to step 3. The pseudo code of step 2 is given in Algorithm 2.

Algorithm 2: Pseudo code of step 2

Let S_s = {all sectionalizing switches in the initial topology}. (*step 2.1*)
Set n_1 and n_2.
Exclude type-1, type-2, and type-3 switches from S_s. (*step 2.2*)
for each switch l in S_s **do** (*step 2.5*)
  Let $\beta_l = 0$ and $\beta_k = 1, \forall k \neq l$. Execute step 1 to obtain a radial topology (β_l is always forced to be 0 during this process). Store the obtained topology. (*step 2.3*)
  Use the obtained topology to calculate the objective via (1) and store the calculated loss. (*step 2.3*)
  Let $\beta_l = 1$. (*step 2.4*)
end for

3) Reasons to Exclude Type-1, Type-2, and Type-3 Switches

Switches near the substation node usually need to be closed/opened such that the nodes near the substation are connected to the substation by the shortest path, i.e., their statuses are relatively easily determined. Therefore, the statuses of switches near the substation in the initial topology usually do not need to be changed. This is why type-1 switches are excluded from S_s in step 2.

Section III-C provides a faster way to change the statuses of type-2 switches in the initial topology and obtain different topologies. Therefore, type-2 switches are excluded from S_s in step 2. The sectionalizing switches that are not in a loop of the original all-switch-closed network cannot be opened; otherwise, some nodes will be isolated. This is the reason to exclude type-3 switches from S_s in step 2.

4) Parallel Framework for Step 2

The 'for' loop in Algorithm 2 can naturally run in parallel. After step 1, the initial topology has been obtained and consequently the S_s used in Algorithm 2 is known. The only input to steps 2.3 and 2.4 is the initial topology and S_s. Therefore, repeating steps 2.3 and 2.4 for different switches (i.e., step 2.5) can run in parallel in different threads or processors. The time given in the simulation part is the longest time consumed by different threads. The maximum number of threads required is the number of switches in S_s. Therefore, excluding type-1, type-2, and type-3 switches from S_s can reduce the maximum number of threads required.

C. Step 3: Change a Sectionalizing Switch Near the Ending Nodes to a Tie Switch

In step 2, the statuses of sectionalizing switches close to the ending nodes, i.e., type-2 switches, in the initial topology are not changed. As a complement, step 3 focuses on changing the statuses of the type-2 switches in the initial topology. The reason for changing the statuses of the type-2 switches in step 3 instead of step 2 is that step 3 is much less time-consuming than step 2. Steps 2 and 3 together can traverse all the sectionalizing switches except type-1 and type-3 switches, i.e., steps 2.5 and 3.4 traverse these switches.

In step 3, the statuses of switches close to ending nodes are changed by opening one switch and closing another switch, which is called the open-1-close-1 (O1C1) approach. In the O1C1 approach, when a closed switch is opened, one and only one downstream node of the opened switch needs to be connected to the network to ensure network connectivity.

Fig. 1 is again used to illustrate the O1C1 approach. For example, switch 6-7 has only one downstream node, i.e., node 7. If branch 6-7 is opened, only one way can ensure connectivity, i.e., connecting node 7 to 8. As another example, switch 22-12 has five downstream nodes, i.e., nodes 12, 13, 14, 11, and 10. If branch 22-12 is opened, two possible ways can ensure connectivity, i.e., connecting node 10 to 9 or connecting node 14 to 15.

For the convenience of expression, four terms are defined in the following.

O1C1 action: opening one switch and closing another in the O1C1 approach is called as an O1C1 action. Note that an O1C1 action changes neither the radiality nor the connectivity of a network.

Objective-decreasing O1C1 action: if an O1C1 action decreases the objective function (1), it is called an objective-decreasing O1C1 action.

Independent feeder: An independent feeder consists of a branch directly connected to the substation node and all of the downstream branches of this branch. Fig. 1 has only one independent feeder, which consists of branch 1-2 and all of the downstream branches.

Independent O1C1 actions: One switch is opened and another closed in an O1C1 action, which involves one or two independent feeders. If none of the feeder(s) involved in one O1C1 action are the same as any of the feeder(s) involved in the other O1C1 action, these two O1C1 actions are called independent O1C1 actions.

A simple and effective strategy to improve the solution accuracy is to combine all independent objective-decreasing O1C1

actions together. This is especially beneficial for a large system with many independent feeders.

The detailed procedure of step 3 is given as follows:

- Step 3.1: For a given radial topology obtained in step 1 or 2, let S_e be a set including all type-2 switches but excluding type-1 and type-3 switches.
- Step 3.2: For a switch l in S_e, find all O1C1 actions that include opening switch l.
- Step 3.3: Execute each O1C1 action found in step 3.2, solve model (1)-(9), and record the objective function after executing this O1C1 action. If this O1C1 action decreases the objective function, then store this action in a set, S_3, which is a set of objective-decreasing O1C1 actions.
- Step 3.4: Repeat steps 3.2-3.3 for different switches in S_e.
- Step 3.5: Combine any two or more independent objective-decreasing O1C1 actions found in steps 3.2-3.4.
- Step 3.6: Repeat steps 3.1-3.5 for different radial topologies obtained in steps 1 and 2.

The pseudo code of step 3 is given in Algorithm 3.

Algorithm 3: Pseudo code of step 3

for each radial topology obtained in steps 1 and 2 **do** (*step 3.6*)
 % The following three lines are step 3.1
 Let S_3={} and S_e={all type-2 switches}.
 Exclude all type-1 and type-3 switches from S_e.
 Obtain the objective via (1), denoted as l_0.

 for each switch l in S_e **do** (*step 3.4*)
 Find all possible O1C1 actions that include opening switch l. (*step 3.2*)
 % The following 'for' loop is step 3.3
 for each O1C1 action **do**
 Solve model (1)-(9) and assign the objective calculated from (1) as a new element to vector L_2.
 Store corresponding network topology.
 if $L_2(l)<l_0$ **then**
 Store the O1C1 action in S_3 that is a set of objective-decreasing actions.
 end if
 end for
 end for
 % The following two-layer 'for' loop is step 3.5
 for each O1C1 action i in set S_3 **do**
 for each O1C1 action j in set S_3 **do**
 if actions i and j are independent from one another **then**
 Combine actions i and j.
 Solve model (1)-(9) and assign the objective calculated from (1) as a new element to vector L_3.
 Store corresponding network topology.
 end if
 end for
 end for
end for
Find the minimum value from l_0, L_2, and L_3, output the corresponding network topology.

Note that step 3.5 in Algorithm 3 combines two independent objective-decreasing O1C1 actions together; this can be extended to combine three or more independent objective-decreasing O1C1 actions by adding deeper layers of 'for' loops. The flowchart of the SOE method has been provided in Fig. 2 for a clear view of its structure.

D. Applicability

The SOE given in Section III can be extended to solve a distribution network planning problem. The reason is that both the planning and the reconfiguration problems can generally be solved by the following steps: 1) close all branches, 2) sequentially opening the branches until a radial network is obtained, and 3) exchange the branch statuses to improve the solution accuracy. Besides, [13] also adopts a heuristic method based on the sequential switch opening and switch exchange, which is similar to the method used in our paper. In [13], the heuristic method has been modified to deal with distributed generation (DG) and prosumer controllable loads. This shows strong evidence that the heuristic method used in our paper can be applied to other problems related to microgrids and active distribution networks. The difference between [13] and our paper is that the former focuses on increasing the solution speed and accommodating DG/controllable loads and the latter focuses on improving the solution accuracy. In summary, the proposed SOE method can be modified to solve other problems such as planning and reconfiguration of microgrids and active distribution networks.

To make our method easily used by both the academia and the industry, the Matlab code of the SOE is available for download at https://github.com/zhanjunpeng/SOE.

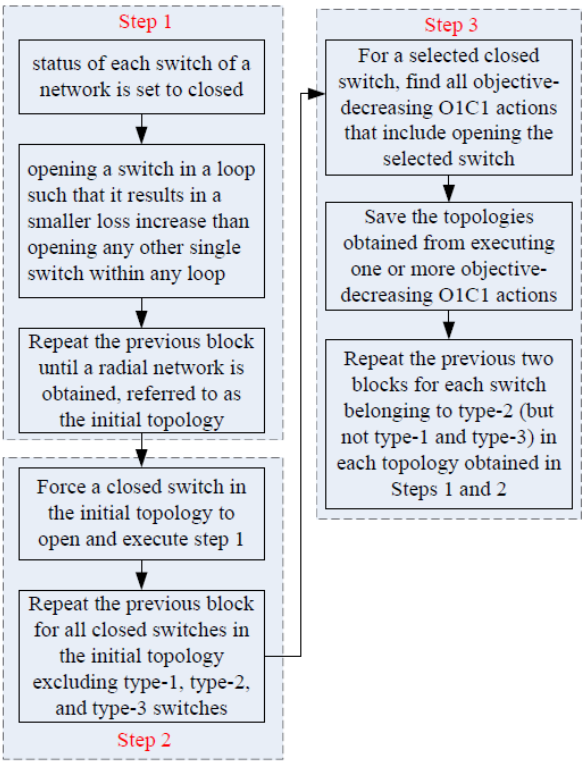

Fig. 2. Flowchart of the SOE method.

IV. Simulation Study

A. Test Systems

To verify the effectiveness of the SOE, the DNR is solved using five different test systems, i.e., 33- and 119-node test systems [33][34], and 84-, 136-, and 417-node test systems [35]. To show the impacts of PV outputs on DNR, three cases of PV

installations are added to the 136-node system as shown in Table I, where the numbers in brackets represent the rated active power of the PV installed and the power factor is set to 0.90. The penetration of PV installation in the three cases is 12.56%, 20.20%, and 30.03%, respectively. The 24-hour profile of the electricity demand (PV output) for a typical summer day used in this paper is obtained from [36] and plotted in Fig. 3a (Fig. 3b). The 24-hour profile is scaled such that its peak load is equal to the system electricity demand of the 136-node system [35]. Hours 9-18 are defined as high-PV periods and hours 1-8 and 19-24 as low-PV periods. The uncertainties of load demand (PV output) are represented by three scenarios, i.e., 0.7, 1.0, and 1.3 times the forecasted load demand (1.0, 0.7, and 0.4 times the PV rating) at probabilities of 0.2, 0.6, and 0.2, respectively. The total number of scenarios is 9, which is equal to the product of the number of load demand scenarios and the number of PV scenarios. Parameters n_1 and n_2, used in both steps 2 and 3 of the SOE, are set to 3 and 2, respectively, to achieve a trade-off between accuracy and computational burden, which will be discussed in Section IV-D. Both MP and SOE are implemented in MATLAB® on a Lenovo® ThinkStation with two Xeon E5-2650 V4 processors.

TABLE I
THREE CASES OF PV INSTALLATION IN THE 136-NODE SYSTEM

Case	Node (values in brackets: rated active power output in kW)
1	89 (800), 107 (1200), 135 (300)
2	89 (1000), 107 (1200), 135 (500), 96 (500), 15 (500)
3	89 (1000), 107 (1200), 135 (500), 96 (500), 15 (500), 52 (500), 132 (500), 35 (500), 83 (300)

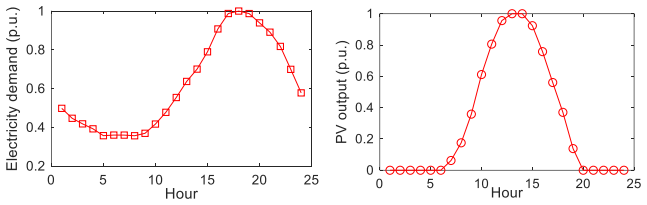

(a) (b)

Fig. 3. 24-hour profiles for a typical summer day: a) electricity demand and b) PV power output.

B. *Comparison Among MP and Different Heuristic Methods*

Table II shows the comparison results between the SOE, MP, and other heuristic algorithms in the literature, including best-first search (BFS) [30], minimum spanning tree (MST) [29], local search (LS) [29], and DISTOP [29]. The minimum loss of the DNR on each system found in the literature and the corresponding time consumption are listed in the 3rd and 4th rows of Table II. The results of the 33-, 84-, and 119-node test systems are taken from [20] and the results of the 136- and 147-node test systems are taken from [27]. Mixed-integer nonlinear programming (MINLP) and mixed-integer linear programming (MILP) are used in [20] and [27], respectively, and they are referred to as MP in this paper. Note that PV output is 0 in each system used in Table II. These minimum losses are marked in bold and used as benchmark values (given in the 3rd row of Table II) to calculate the relative errors, in round brackets, between the losses obtained by different methods and the benchmark values. The relative error used in Tables II and IV is defined as $(x - x_b)/x_b$ where x is the loss obtained by a method and x_b is the benchmark (i.e., the value in bold in Table II).

To verify the optimality of the SOE on the 33-node system, a brute-force search as described below is performed for the 33-node system. The brute-force search for other systems is computationally intractable and, therefore, is not performed. The 33-bus system has 37 branches and 33 buses. In order to achieve a radial network, there should be 32 sectionalizing branches and 5 tie branches. All branches in the network are closed and 5 different branches are opened; this results in 52,836 connected networks. Among the 52,836 connected networks, 2,085 have loops and 50,751 are radial. The power flow of each of the 50,751 radial networks is solved and the minimal loss is 139.55 kW and the corresponding radial network is exactly the same as the one shown in Fig. 1. As shown in row 14 of Table IV, the first step of SOE already finds the optimal solution of the 33-node system, i.e., the minimal loss is 139.55 kW, which verifies the effectiveness of the SOE.

Table II shows that the accuracy of the SOE is 99.71%-100% in different single-hour DDNR problems, i.e., the SOE is accurate in both small and large systems. The MP, BFS, DISTOP, and SOE have obtained the optimal solution in the 33-node system but MST and LS do not. As shown in Table II, SOE is better than the other four heuristic methods in all the 84-node, 119-node, 136-node, and 417-node systems. SOE is 5.36% and 5.34% better than BFS and DISTOP in the 136-node system, respectively, and is 13.61% and 12.31% better than MST and LS in the 417-node system, respectively. Thus, it is clear that SOE obtains more accurate results than all the other four heuristic methods.

We have implemented the MST and LS methods and obtained the same losses as [29] on the 33-node, 84-node, and 119-node systems but obtained much larger loss on the 136-node system than the loss given in [29]. So, the loss values obtained by MST and LS on the 136-node system are taken from [29]. The loss on the 417-node system obtained by the MST and LS methods is generated from our code as the 417-node system was not used in [29]. The results of DISTOP are taken from [29] and we do not implement DISTOP. Therefore, the result of the 417-node system is not shown as it is not available in [29].

TABLE II
RESULTS OF THE ONE-HOUR DNR OBTAINED BY MP AND FIVE DIFFERENT HEURISTIC ALGORITHMS ON THE FIVE TEST SYSTEMS (NUMBER IN BRACKETS REPRESENTS RELATIVE ERROR TO BENCHMARK).

Method		Test systems				
		33-node	84-node	119-node	136-node	417-node
MP	Loss (kW)	**139.55**	**469.88**	**853.58**	**280.14**	**581.57**
	Time (s)	19	3030	4007	1236	171425
BFS [30]	Loss (kW)	139.55	471.45	874.83	295.97	595.33
	(R. error)	(0%)	(0.33%)	(2.49%)	(5.65%)	(2.37%)
MST [29]	Loss (kW)	140.7	471.7	894.3	289.4	662.50
	(R. error)	(0.8%)	(0.39%)	(4.77%)	(3.31%)	(13.9%)
LS [29]	Loss (kW)	139.9	470.08	883.5	286.4	654.84
	(R. error)	(0.3%)	(0.34%)	(3.51%)	(2.23%)	(12.6%)
DISTOP [29]	Loss (kW)	139.55	471.4	891.9	295.9	-
	(R. error)	(0%)	(0.32%)	(4.49%)	(5.63%)	-
SOE	Loss (kW)	139.55	470.06	853.58	280.94	582.86
	(R. error)	(0%)	(0.04%)	(0%)	(0.29%)	(0.22%)
	Time (s)	1	6.2	12.3	16.9	265.4

The BFS takes 32 seconds to solve a system with 129 switches as given in [30]; the MST and LS take 0.023 and 0.261 seconds to solve a 119-node system, respectively; the DISTOP takes 90 seconds to solve a system with 512 switches. That is, the BFS, MST, LS, and DISTOP are fast and not time-consuming. The topology solution in terms of tie switches of the single-hour DDNR obtained by the SOE on each test system is tabulated in Table III.

The MP, BFS, and SOE are used to solve the 24-hour DDNR on the 136-node system and the losses of the solutions obtained by these three methods are 3517.8, 3093.4, and 2940.0 kW, respectively. The 24-hour DNR problem on the136-node system was converted into an MILP model based on [37]. The MILP was solved by CPLEX for 24 hours but does not converge, and the loss associated with its solution is 19.65% higher than the SOE; this indicates that the MP is incapable of solving the large-scale multi-hour DDNR. The reason is that a multi-hour DDNR has many more binary and continuous variables as well as constraints than a single-hour DDNR and is therefore much more difficult to solve.

The last row of Table II shows that the SOE is fast, which is especially beneficial for solving a large-scale multi-hour DDNR. For example, the MP method requires 1,236 and 86,400 seconds to solve the single-hour and 24-hour DDNR in the 136-node system while the SOE requires only 16.9 and 265.4 seconds, which is 72 and 325 times faster than the MP, respectively. Therefore, the SOE is accurate, fast, and superior to the MP and other heuristic algorithms compared, especially for solving a large-scale multi-hour DDNR.

TABLE III
TIE SWITCHES OF THE SINGLE-HOUR DDNR RESULT OBTAINED BY THE SOE USING THE FIVE TEST SYSTEMS.

Systems	Tie switches
33-node	7-8, 9-10, 14-15, 32-33, 25-29
84-node	6-7, 12-13, 33-34, 38-39, 41-42, 54-55, 62-63, 71-72, 82-83, 11-43, 14-18, 16-26, 28-32
119-node	23-24, 25-26, 35-36, 41-42, 44-45, 52-53, 61-62, 74-75, 77-78, 95-100, 101-102, 114-115, 56-45, 113-86, 110-89
136-node	6-7, 8-9, 31-35, 48-51, 53-54, 89-90, 95-96, 105-106, 104-118, 125-126, 134-135, 15-83, 50-96, 66-79, 79-131, 84-135, 91-104, 90-129, 92-104, 92-132, 128-77
417-node	66-384, 382-66, 221-220, 75-81, 68-85, 27-31, 60-58, 275-209, 34-47, 257-259, 77-59, 58-20, 41-43, 383-370, 20-33, 95-112, 7-3, 281-235, 281-282, 105-108, 46-42, 21-49, 39-30, 293-236, 107-103, 304-306, 10-11, 84-99, 3-10, 21-57, 314-317, 310-315, 310-305, 129-346, 142-136, 160-181, 133-140, 202-1, 144-148, 143-150, 145-146, 173-179, 179-160, 149-138, 290-289, 265-266, 243-249, 319-318, 303-304, 305-308, 311-304, 260-324, 334-336, 381-268, 336-337, 323-322, 234-233, 296-295, 230-228

C. Impacts of Different Steps in the SOE

To illustrate the effectiveness of each step in the SOE, the DNR on each system is solved by the SOE with all the three steps, with only steps 1 and 2, with only steps 1 and 3, with only step 1; the power losses and relative error of the obtained solutions and time consumption are given in rows 5-7, 8-10, 11-13, and 14-16 of Table IV, respectively. The results of MP are shown again in Table IV as they are used as the benchmark values to calculate the relative errors.

Comparing the 10th, 13th, and 16th rows of Table IV shows that steps 1 and 2 are relatively time-consuming while step 3 consumes little time. The 15th row of Table IV reveals that step 1 is sufficient to obtain an accurate solution of small test systems (relative errors in the 33- and 84-node systems are 0 and 0.33%, respectively) but insufficient for larger test systems (relative errors in the 119-, 136-, and 417-node systems are 2.49%, 5.65%, and 2.37%, respectively).

This paragraph focuses on the three large systems, i.e., the last three columns of Table IV. Comparing rows 9 and 15 shows that adding step 2 to step 1 can reduce the relative errors from 2.49%, 5.65%, and 2.37% to 0.05%, 1.17%, and 0.86% for the 119-, 136-, and 417-node system, respectively. This shows the effectiveness of step 2. Comparing the 9th, 12th, and 15th rows indicates that step 2 can better reduce the system loss than step 3. Comparing the 6th and 9th rows of Table IV reveals that adding step 3 to steps 1 and 2 can further reduce the system loss, which is recommended as step 3 consumes little time as mentioned in the previous paragraph.

TABLE IV
LOSSES (KW) OF THE DNR OBTAINED BY MP AND SOE WITH DIFFERENT STEPS ON THE FIVE TEST SYSTEMS AND THE TIME CONSUMPTION (NUMBER IN BRACKETS REPRESENTS RELATIVE ERROR).

Method	R		Test systems				
			33-node	84-node	119-node	136-node	417-node
MP	3	Loss	**139.55**	**469.88**	**853.58**	**280.14**	**581.57**
	4	Time (s)	19	3030	4007	1236	171425
SOE with steps 1+2+3	5	Loss	139.55	470.06	853.58	280.94	582.86
	6	(R. error)	(0%)	(0.04%)	(0%)	(0.29%)	(0.22%)
	7	Time (s)	1.0	6.2	12.3	16.9	265.4
SOE with steps 1+2	8	Loss	139.55	471.45	854.03	283.43	586.56
	9	(R. error)	(0%)	(0.33%)	(0.05%)	(1.17%)	(0.86%)
	10	Time (s)	0.9	5.6	11.9	15.5	252.1
SOE with steps 1+3	11	Loss	139.55	470.89	872.89	288.82	589.69
	12	(R. error)	(0%)	(0.21%)	(2.26%)	(3.10%)	(1.40%)
	13	Time (s)	0.7	3.3	6.4	11.2	157.1
SOE with step 1	14	Loss	139.55	471.45	874.83	295.97	595.33
	15	(R. error)	(0%)	(0.33%)	(2.49%)	(5.65%)	(2.37%)
	16	Time (s)	0.6	3.0	5.5	8.1	132.3

Step 3 consists of O1C1 actions and combining n independent objective-decreasing O1C1 actions together where n is a natural number and $n \geq 2$. Here the SOE with three versions of step 3 is used (referred to as SOE1, SOE2, and SOE3, respectively) to investigate the impacts of different components within step 3. In each of SOE1, SOE2, and SOE3, SOE with all steps 1, 2, and 3 is used and the difference among them lies in step 3 as detailed below:

- SOE1: step 3 only consists of O1C1 actions.
- SOE2: step 3 only consists of combining two independent objective-decreasing O1C1 actions together.
- SOE3: step 3 only consists of combining three independent objective-decreasing O1C1 actions together.

The three versions of SOE are used to solve each test system (33-bus system is excluded as step 1 of SOE already obtains the optimum solution) with the results tabulated in Table V. The minimum loss in each test system is marked in bold. The 84- and 119-node systems do not have three independent objective-decreasing O1C1 actions as these two systems are relatively

small. Table V shows that the minimum solution can come from each of SOE1, SOE2, and SOE3. For a large system such as the 417-node system, step 3 can be set to combine more independent objective-decreasing O1C1 actions to find a better solution. In general, step 3 is recommended to consist of O1C1 actions and combining n independent objective-decreasing O1C1 actions ($n = 2$ and 3).

TABLE V
LOSSES (KW) OF THE DNR OBTAINED BY SOE WITH DIFFERENT VERSIONS OF STEP 3.

SOE	Test systems			
	84-node	119-node	136-node	417-node
SOE1	470.09	**853.58**	281.17	584.20
SOE2	**470.06**	862.26	**280.94**	582.92
SOE3	---	---	281.25	**582.86**

D. Sensitivity Analysis of the SOE

This subsection investigates the impacts of the setting of two parameters, i.e., n_1 and n_2, used in both steps 2 and 3 of the SOE. They are the only two parameters in the SOE. The best solution for the 33-node system is obtained in step 1 of the SOE. Therefore, only the other four systems, i.e., the 84-, 119-, 136-, and 417-node systems, are used to analyze the impacts of the setting of n_1 and n_2. The one-hour DNR is solved by the SOE on the four systems using different settings of n_1 and n_2 and the results are tabulated in Table VI. As the values of n_1 and n_2 increase, the number of elements left in S_s in step 2 decreases. An empty S_s is equivalent to not implement step 2. The value of n_1 or n_2 are not increased to a value such that S_s becomes empty. This is why some results in Tables VI and VII related to large values of n_1 and n_2 are empty and marked as '--'. Besides, after the power loss becomes increasing as the increase of n_1 (n_2), the results are not used and, therefore, not provided and marked as '--'.

The minimum values obtained in each system are marked in bold in both Tables VI and VII. Table VI shows that as n_1 increases from 0 to 3 (7, 5, 6) and n_2 is fixed to 2, the power loss of the 84-node (119-node, 136-node, 417-node) system does not increase and is equal to the minimum value obtained by the SOE; but the power loss increases as n_1 further increases. Table VI also shows that the maximum number of threads required (i.e., the numbers in brackets) decreases as n_1 increases. For the 84-node system, n_1 is recommended to be 3 to achieve a trade-off between accuracy and computational burden. For larger systems (i.e., the 119-, 136-, 417-node systems), n_1 can be set to 5 to achieve a lower computational burden without degrading accuracy.

Table VII shows that as n_2 increases from 0 to 2 and n_1 is fixed to 3, the power losses of the 84-, 119-, and 136-node systems do not increase and are equal to the minimum values obtained by the SOE; but the power losses increase as n_2 further increases. For the 417-node system, the optimal value of n_2 is 2-3 as shown in Table VII. Besides, Table VII shows that the maximum number of threads required (i.e., the numbers in brackets) decreases significantly as n_2 increases. Setting n_2 to a large value can reduce the computational burden but the accuracy of the SOE will decrease when n_2 is too large. According to Table VII, n_2 can be set to 2 to achieve a trade-off between accuracy and computational burden.

TABLE VI
THE POWER LOSS OF THE DNR OBTAINED BY THE SOE WITH DIFFERENT SETTINGS OF n_1 (n_2 FIXED TO 2) AND THE NUMBERS IN BRACKETS REPRESENT THE MAXIMUM NUMBER OF THREADS REQUIRED.

n_1	84-node sys.	119-node sys.	136-node sys.	417-node sys.
0	**470.058 (25)**	**853.58 (55)**	**280.94 (24)**	**582.8573 (100)**
1	**470.058 (16)**	**853.58 (50)**	**280.94 (21)**	**582.8573 (96)**
2	**470.058 (8)**	**853.58 (43)**	**280.94 (18)**	**582.8573 (87)**
3	**470.058 (3)**	**853.58 (35)**	**280.94 (14)**	**582.8573 (71)**
4	471.445 (1)	**853.58 (24)**	**280.94 (11)**	**582.8573 (58)**
5	--	**853.58 (15)**	**280.94 (10)**	**582.8573 (51)**
6	--	**853.58 (9)**	281.17 (8)	**582.8573 (47)**
7	--	**853.58 (6)**	283.5 (4)	584.472 (41)
8	--	874.83 (3)	--	--

TABLE VII
THE POWER LOSS OF THE DNR OBTAINED BY THE SOE WITH DIFFERENT SETTINGS OF n_2 (n_1 FIXED TO 3) AND THE NUMBERS IN BRACKETS REPRESENT THE MAXIMUM NUMBER OF THREADS REQUIRED.

n_2	84-node sys.	119-node sys.	136-node sys.	417-node sys.
0	**470.058 (21)**	**853.58 (67)**	**280.94 (50)**	585.09 (196)
1	**470.058 (9)**	**853.58 (51)**	**280.94 (30)**	584.473 (126)
2	**470.058 (3)**	**853.58 (35)**	**280.94 (14)**	**582.8573 (71)**
3	471.4456 (1)	854.034 (20)	285.88 (4)	**582.8573 (37)**
4	--	854.034 (9)	295.966 (1)	583.944 (22)
5	--	874.83 (4)	--	589.9843 (12)

In the SOE described in Algorithms 1-3, changing the statuses of the type-2 switches is excluded from step 2 and included only in step 3. It is interesting to investigate whether it would be better to change the statuses of the type-2 switches in step 2 instead of in step 3. For the convenience of expression, a revised SOE is defined as: it consists of Algorithms 1-3 where step 2.2 is modified as 'Exclude type-1 and type-3 switches from S_s'. That is, the revised SOE lets step 2 handle type-2 switches instead of step 3. Both versions are used to solve the four test systems and the results show that the revised SOE obtains the same optimal solution in each test system as the SOE. However, the revised SOE has 21, 67, 50, and 196 elements in S_s while the SOE has 3, 35, 14, and 71 elements in S_s in step 2.5, i.e., the former needs more threads in step 2 than the latter. In summary, the revised SOE has a higher computational burden than the SOE but obtains the same optimal solution. Thus, SOE is recommended instead of the revised SOE.

E. Comparison Between Single-hour and Multi-hour DNRs

In this subsection, DNR refers to both DDNR and SDNR. The single-hour, 24-hour DNRs, and the multi-hour DNR in the low and high PV periods are solved and the topology results obtained are referred to as topology-1, topology-24, topology-low, and topology-high, respectively. The per-hour loss associated with topology-24, topology-low, and topology-high are referred to as loss-24, loss-low, and loss-high, respectively, where the per-hour loss is calculated from (1) divided by the number of hours.

Loss-1 is also a per-hour loss but is calculated differently as follows. The relative errors between loss-1 and each of loss-24, loss-low, and loss-high for each of cases 1-3 is given in the 3rd, 4th, and 5th columns of Table VIII, respectively. For a fair comparison, in each of the 3rd, 4th, and 5th columns in Table III, two different topologies are compared using the same load and PV. For example, topology-24 and topology-1 are used in the 3rd column and loss-1 in this column is obtained from running AC power flow on topology-1 using the 24-hour load/PV used in the 24-hour DNRs. Similarly, loss-1 in the 4th and 5th columns is associated with topology-1 using the load/PV in the low-PV and high-PV periods (defined in Section IV-A), respectively.

In Sections IV-E, IV-F, IV-G, and IV-H, 136-node test system is used. The comparisons for both DDNRs and SDNRs have been performed and the results related to the DDNRs and SDNRs are listed in the 2nd-4th, 5th-7th rows of Table VIII, respectively. The negative values in Table VIII indicate that topology-1 results in higher loss than topology-24, topology-low, and topology-high. The positive values will be explained below.

Topology-1 is a feasible solution of (1)-(11), i.e., it does not have voltage violation, for the same load/PV value used in the single-hour DNR. However, topology-1 can be infeasible when using other values of load and PV as described above. For the results related to DDNRs, topology-1 violates voltage upper limit in several low-load high-PV hours in cases 2 and 3. For the results related to SDNRs, topology-1 violates the voltage upper limit in all cases 1-3. This is why the relative error marked in bold in Table VIII is positive, i.e., topology-1 results in a low loss at the cost of voltage violation.

The 4th column of Table VIII shows that loss-low is the same as loss-1 for DDNRs while the loss-low is lower than loss-1 for SDNRs. The 3rd (5th) column of Table VIII indicates that loss-24 (loss-high) is lower than loss-1 if topology-1 does not experience a voltage violation but higher than loss-1 if topology-1 experiences a voltage violation. To illustrate the voltage violation, the nodal voltage profile at hour 12 for the topology obtained from the single-hour DDNR is shown in Fig. 4, where the voltage upper limit (1.05) is violated at 37 nodes. Note that hour 12 is involved in both the 24-hour DDNR and the multi-hour DDNR in the high PV periods.

In summary, when the PV output is high (low), solving the multi-hour DDNR can (cannot) obtain lower losses than solving the single-hour DDNR. Solving the multi-hour SDNR instead of single-hour SDNR can avoid voltage violation and achieve lower losses when the PV output is high and low, respectively. Therefore, it is better to solve the multi-hour DNRs to obtain lower losses or avoid violating voltage limits compared to solving single-hour DNRs.

TABLE VIII
THE RELATIVE ERROR BETWEEN THE PER-HOUR LOSSES OF THE MULTI-HOUR AND SINGLE-HOUR DDNRS/SDNRS SOLVED BY THE SOE

	Case	Loss-24 vs. loss-1*	Loss-low vs. loss-1	Loss-high vs. loss-1
DDNR	1	-1.11%	0.0%	-4.51%
	2	-0.32%	0.0%	-9.26%
	3	**4.12%**	0.0%	-4.65%
SDNR	1	**14.11%**	-1.56%	**11.34%**
	2	**26.15%**	-4.23%	**24.65%**
	3	**57.81%**	-3.91%	**55.76%**

* The relative error of lossA vs. lossB is calculated as (lossA-lossB)/lossB

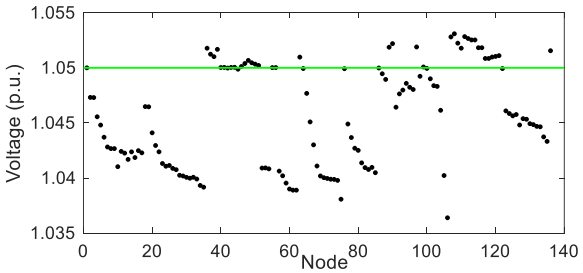

Fig. 4. The nodal voltage for the topology obtained from the single-hour DDNR using the load demand and PV output at hour 12.

F. Comparison of Hourly, 24-hour, and Block DNRs

In this subsection, DNR refers to both DDNR and SDNR. As explained in the Introduction, the hourly DNR solves a single-hour DNR for each hour of a day independently. The 24-hour DNR refers to (1)-(11), with Ω_s having only one element and $T = 24$. The block DNR refers to solving the multi-hour DNRs in the low-PV and high-PV periods separately and combining their results. The results, in terms of total losses and total number of switching actions within 24 hours, of the hourly DNR, 24-hour DNR, and block DNR are tabulated in Table IX. Table IX shows that the hourly DNR has the lowest loss: the 24-hour loss of the 24-hour (block) DDNR is 1.95%, 4.75%, and 8.57% (1.08%, 1.40%, and 2.45%) higher than the hourly DDNR in cases 1-3, respectively; the 24-hour loss of the 24-hour (block) SDNR is 14.8%, 28.6%, 58.1% (9.1%, 14.6%, and 34.7%) higher than the hourly SDNR in cases 1-3, respectively.

However, the result of hourly DNR has a large number of switching actions (i.e., 86, 142, and 178 for DDNR and 114, 150, and 188 for SNDRs in cases 1-3, respectively), which is much higher than the block DNR (i.e., 16, 20, and 40 for DDNR and 10, 20, and 30 for SDNR in cases 1-3, respectively). Note that the topology result of the 24-hour DNR remains the same within a day and therefore, the number of switching actions is zero. Comparing columns 4-6 of Table IX indicates that the result of the block DDNR/SDNR can achieve a good trade-off between loss and the number of switching actions, which is recommended.

TABLE IX
COMPARISON AMONG HOURLY, 24-HOUR, AND BLOCK DNRS

	Case		Hourly	24-hour	Block
DD NR	1	24-hour loss in kWh	2342.4	2388.0 (1.95%)*	2367.8 (1.08%)
		No. swit. actions	86	0	16
	2	24-hour loss in kWh	2172.0	2275.2 (4.75%)	2202.4 (1.40%)
		No. swit. actions	142	0	20
	3	24-hour loss in kWh	1987.2	2157.6 (8.57%)	2035.8 (2.45%)
		No. swit. actions	178	0	40
SD NR	1	24-hour loss in kWh	2553.1	2930.4 (14.8%)	2785.2 (9.1%)
		No. swit. actions	114	0	12
	2	24-hour loss in kWh	2437.1	3134.4 (28.6%)	2792.7 (14.6%)
		No. swit. actions	150	0	20
	3	24-hour loss in kWh	2333.9	3688.8 (58.1%)	3142.9 (34.7%)
		No. swit. actions	188	0	30

* The numbers in brackets represent relative errors that are calculated as (x-x0)/x0, where x is a loss given in the 5th or 6th column and x0 is given in the 4th column and the same row as x.

G. Comparison Between DDNR and SDNR

In this subsection, 24-hour DDNRs and SDNRs using the 136-node system are solved and compared. For the purpose of

comparison, the topologies obtained from both the DDNRs and SDNRs are used to calculate the total system losses in a day and AC power flow is run to obtain the nodal voltage for each hour under different load and PV scenarios.

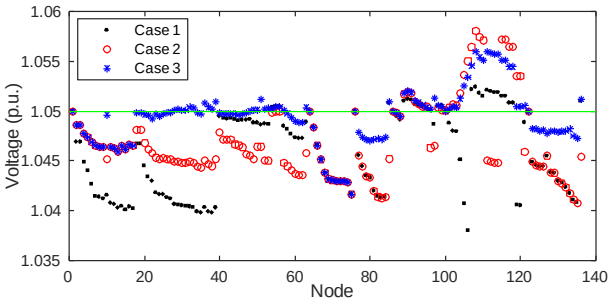

Fig. 5. The nodal voltage for the topology result obtained from the DDNR in the low-load high-PV scenario of hour 12 in cases 1-3.

As each hour in each scenario is considered in the SDNR model, the solution of the SDNR satisfies the voltage constraint (5) at each node, each hour, and each scenario. However, the results of the DDNR for some low-load and high-PV scenarios/hours violate the voltage upper limit. For each of cases 1-3, the nodal voltage for the scenario/hour with the highest voltage violation is shown in Fig. 5; this scenario/hour is the low-load high-PV scenario in hour 12 for each case. Note that only the result of DDNR is shown in Fig. 5; the result of SDNR is not shown as it has no voltage violation. Fig. 5 shows that the voltage violating its upper limit, 1.05, is severe from nodes 104 to 120, and cases 2 and 3 have more severe voltage violations than case 1. As shown in Fig. 5, 27, 26, and 56 nodes in cases 1-3, respectively, violate the voltage upper limit. In summary, as the PV penetration increases, more nodes are likely to violate the voltage upper limit to a greater extent for the topology obtained from the DDNR. Therefore, solving the SDNR is superior to solving the DDNR.

H. Number of Scenarios in 24-hour SDNR

The number of scenarios in stochastic programming is an important parameter. This subsection investigates the impacts of using different numbers of scenarios. In this subsection, the uncertainties of load demand (PV output) are represented by seven scenarios, i.e., 0.7, 0.8, 0.9, 1.0, 1.1, 1.2, and 1.3 times the forecasted load demand (0.4, 0.5, 0.6, 0.7, 0.8, 0.9, and 1.0 times the PV rating). Different load scenarios are combined with different PV scenarios, i.e., 49 scenarios are obtained, which is equal to the product of the number of load demand scenarios and the number of PV scenarios. To model the uncertainty, the 49 scenarios of load and PV data are used to generate new data by multiplying a random number. Specifically, each element of the data is multiplied by a random number between 0.9 and 1.1. This process repeats 10 times and generates 10 new sets of 49 scenarios. The total number of scenarios now becomes 49+490, i.e., 539. Using many scenarios in stochastic programming can be computationally intractable. Therefore, a scenario reduction method, e.g., improved forward selection algorithm [38], is usually used to reduce the many scenarios to a relatively small number of representative scenarios. Here, 10, 50, and 100 representative scenarios are used, referred to as cases 4, 5, and 6, respectively. Note that instead of using the original scenarios, only the representative scenarios are used in model (1)-(11).

The simulation results are tabulated in Table X including losses and time consumptions. The time consumption listed in the last column of Table X includes step 1, step 3, and the most time-consuming thread in step 2. As shown in Table X, the number of representative scenarios in cases 5 and 6 is 5 and 10 times of case 4, respectively. The time associated with cases 5 and 6 is about 4.8 and 9.2 times of case 4, respectively. That is, the time consumption of the SOE method increases linearly as the number of representative scenarios increases. It is well known that the computational burden of using MP methods to solve a stochastic programming problem increases exponentially as the increase in the number of representative scenarios. Thus, the SOE is superior to MP methods in terms of both computational burden and accuracy in solving SDNRs.

Although the solution time of SOE increases linearly, the time consumption in cases 5 and 6 is long, especially if only a few threads are used in step 2 of the SOE to solve the SDNR in parallel. Table X shows that the objective functions, i.e., the loss, obtained by the three cases are close to one another. Therefore, it is recommended to use a relatively small number of representative scenarios to shorten solution time.

TABLE X
TIME CONSUMPTION AND 24-HOUR LOSS OF THE 24-HOUR SDNR SOLVED BY THE SOE USING DIFFERENT NUMBERS OF REPRESENTATIVE SCENARIOS

Case	Number of representative scenarios	Loss (kW)	Time consumption (s)
4	10	2073.6	3147
5	50	2102.4	15256
6	100	2102.4	28957

V. CONCLUSION

A multi-hour SDNR is proposed to handle variable and uncertain load and PV output. Existing methods for SDNR are either inaccurate or too time-consuming. Thus, an accurate and fast heuristic method, SOE, is proposed to solve both the SDNR and DDNR. The SOE consists of three steps. The first step can obtain a relatively accurate initial solution fast and the second and third steps further improve the accuracy.

The simulation results show that the SOE 1) is more accurate than the other heuristic methods compared, 2) is almost as accurate (99.71%-100%) as the MP in single-hour DDNRs, and 3) is much better (e.g., 19.65% less loss) than the MP in solving multi-hour DDNRs. The solution speed of the SOE is significantly faster (e.g., 72-2325 times faster) than the MP. Therefore, the SOE is superior, in terms of accuracy and/or solution speed, to MP and the other heuristic methods compared, especially in solving large-scale multi-hour DDNRs. The simulation results also show that 1) solving the multi-hour DDNR/SDNR can obtain better results, i.e., having lower losses and/or satisfying voltage limits, than solving the single-hour DDNR/SDNR, 2) block DDNR/SDNR can achieve a good trade-off between loss and number of switching actions while hourly DDNR/SDNR has many switching actions and 24-hour DDNR/SDNR has a high loss, and 3) the SDNR is superior to the DDNR as the result obtained from the DDNR can violate the voltage upper limit when the load (PV output) is lower (higher) than its predicted value.

REFERENCES

[1] F. Capitanescu, L. F. Ochoa, H. Margossian, and N. D. Hatziargyriou, "Assessing the potential of network reconfiguration to improve distributed generation hosting capacity in active distribution systems", *IEEE Trans. Power Syst.*, vol. 30, no. 1, pp. 346-356, Jan. 2015.

[2] J. P. Chiou, C. F. Chang, and C. T. Su, "Variable scaling hybrid differential evolution for solving network reconfiguration of distribution systems", *IEEE Trans. Power Syst.*, vol. 20, no. 2, pp. 668-674, May 2005.

[3] Y. Liu, J. Li, and L. Wu, Coordinated Optimal Network Reconfiguration and Voltage Regulator/DER Control for Unbalanced Distribution Systems, *IEEE Trans. Smart Grid*, vol. 10, no. 3, pp. 2912-2922, 2019.

[4] A. Arif, Z. Wang, J. Wang, and C. Chen, Power Distribution System Outage Management With Co-Optimization of Repairs, Reconfiguration, and DG Dispatch, *IEEE Trans. Smart Grid*, vol. 9, no. 5, pp. 4109-4118, 2018.

[5] C. Lee, C. Liu, S. Mehrotra, and Z. Bie, Robust Distribution Network Reconfiguration, *IEEE Trans. Smart Grid*, vol. 6, no. 2, pp. 836-842, 2015.

[6] Z. C. Li, S. Jazebi, and F. D. Leon, "Determination of the optimal switching frequency for distribution system reconfiguration", *IEEE Trans. Power Del.*, vol. 32, no. 4, pp. 2060-2069, Aug. 2017.

[7] International Energy Agency. (2014). Technology Roadmap: Solar Photovoltaic Energy. [Online]. Available: https://www.iea.org.

[8] C. Peng, L. Xu, X. Gong, H. Sun and L. Pan, "Molecular evolution based dynamic reconfiguration of distribution networks with DGs considering three-phase balance and switching times," *IEEE Trans. Industrial Informatics*, vol. 15, no. 4, pp. 1866-1876, April 2019.

[9] A. Arif, Z. Wang, J. Wang and C. Chen, "power distribution system outage management with co-optimization of repairs, reconfiguration, and DG dispatch," *IEEE Trans. Smart Grid*, vol. 9, no. 5, pp. 4109-4118, Sept. 2018.

[10] Y. Takenobu, N. Yasuda, S. Kawano, S. Minato, and Y. Hayashi, "Evaluation of annual energy loss reduction based on reconfiguration scheduling," *IEEE Trans. Smart Grid*, vol. 9, no. 3, pp. 1986-1996, May 2018.

[11] H. Wang, W. Zhang, and Y. Liu, "A robust measurement placement method for active distribution system state estimation considering network reconfiguration," *IEEE Trans. Smart Grid*, vol. 9, no. 3, pp. 2108-2117, May 2018.

[12] J. Singh and R. Tiwari, "Real power loss minimisation of smart grid with electric vehicles using distribution feeder reconfiguration," *IET Generation, Transmission & Distribution*, vol. 13, no. 18, pp. 4249-4261, 2019.

[13] R. A. Jabr, I. Džafić, and I. Huseinagić, "Real time optimal reconfiguration of multiphase active distribution networks," *IEEE Trans. Smart Grid*, vol. 9, no. 6, pp. 6829-6839, Nov. 2018.

[14] V. Roberge, M. Tarbouchi and F. A. Okou, "Distribution system optimization on graphics processing unit," *IEEE Trans. Smart Grid*, vol. 8, no. 4, pp. 1689-1699, July 2017.

[15] A. G. Fonseca, O. L. Tortelli, and E. M. Lourenço, "Extended fast decoupled power flow for reconfiguration networks in distribution systems," *IET Generation, Transmission & Distribution*, vol. 12, no. 22, pp. 6033-6040, 2018.

[16] S. Khodayifar, M. A. Raayatpanah, A. Rabiee, H. Rahimian, and P.M. Pardalos, "Optimal long-term distributed generation planning and reconfiguration of distribution systems: an accelerating Benders' decomposition approach," *J. Optimization Theory Applications*, vol. 179, pp. 283–310, 2018.

[17] H. M. Khodr, J. Martınez-Crespo, Z.A. Vale, and C. Ramos, "Optimal methodology for distribution systems reconfiguration based on OPF and solved by decomposition technique," *Euro. Trans. Electr. Power*, vol. 20, pp. 730-746, 2010.

[18] E. R. Ramos, A. G. Expósito, J. R. Santos, and F. L. Iborra, "Path-based distribution network modeling: application to reconfiguration for loss reduction", *IEEE Trans. Power Syst.*, vol. 20, no. 2, pp. 556-564, May 2005.

[19] A. Asrari, T. Wu, and S. Lotfifard, "The impacts of distributed energy sources on distribution network reconfiguration", *IEEE Trans. Energy Convers.*, vol. 31, no. 2, pp. 606-613, Jun. 2016.

[20] M. Lavorato, J. F. Franco, M. J. Rider, and R. Romero, "Imposing radiality constraints in distribution system optimization problems", *IEEE Trans. Power Syst.*, vol. 27, no. 1, pp. 172-180, Feb. 2012.

[21] F. Ding and K. A. Loparo, "Hierarchical Decentralized Network Reconfiguration for Smart Distribution Systems - Part II: Applications to Test Systems," *IEEE Trans. Power Syst.*, vol. 30, no. 2, pp. 744-752, 2015.

[22] R. A. Jabr, R. Singh, and B. C. Pal, "Minimum loss network reconfiguration using mixed-integer convex programming", *IEEE Trans. Power Syst.*, vol. 27, no. 2, pp. 1106-1115, May 2012.

[23] Z. Guo, S. Lei, Y. Wang, Z. Zhou, and Y. Zhou, "Dynamic distribution network reconfiguration considering travel behaviors and battery degradation of electric vehicles", in *IEEE PES General Meeting*, Chicago, U.S.A., 2017, pp. 1-5.

[24] H. Haghighat and B. Zeng, "Distribution system reconfiguration under uncertain load and renewable generation", *IEEE Trans. Power Syst.*, vol. 31, no. 4, pp. 2666-2675, 2016.

[25] C. Lee, C. Liu, S. Mehrotra, and Z. Bie, "Robust Distribution network reconfiguration", *IEEE Trans. Smart Grid*, vol. 6, no. 2, pp. 836-842, 2015.

[26] P. Zhang, W.Y. Li, and S.X. Wang, "Reliability-oriented distribution network reconfiguration considering uncertainties of data by interval analysis", *Int. J. Electric Power Energy Syst*, vol. 34, pp. 138-144, 2012.

[27] M. C. O. Borges, J. F. Franco, and M. J. Rider, "Optimal reconfiguration of electrical distribution systems using mathematical programming", *J. Control Autom. Electr. Syst.*, vol. 25, pp. 103-111, 2014.

[28] J. F. Franco, M. J. Rider, M. Lavorato, and R. Romero, "A mixed-integer LP model for the reconfiguration of radial electric distribution systems considering distributed generation", *Elect. Power Syst. Res.*, vol. 97, pp. 51-60, 2013.

[29] H. Ahmadi and J.R. Marti, "Minimum-loss network reconfiguration: A minimum spanning tree problem", *Sustainable Energy, Grids and Networks*, vol. 1, pp. 1-9, 2015.

[30] H.P. Schmidt, N. Ida, N. Kagan, and J. C. Guaraldo, "Fast reconfiguration of distribution systems considering loss minimization", *IEEE Trans. Power Syst.*, vol. 20, no. 3, pp. 1311-1319, Aug. 2005.

[31] S. Mishra, D. Das, and S. Paul, A comprehensive review on power distribution network reconfiguration, Energy Syst., vol. 8, no. 2, pp. 227-284, 2017.

[32] Y. Liu, J. Bebic, B. Kroposki, J. D. Bedout, and W. Ren, "Distribution system voltage performance analysis for high-penetration PV", IEEE Energy 2030, Atlanta, Georgia, USA, Nov. 2008.

[33] R. Seguin, J. Woyak, D. Costyk, J. Hambrick, and B. Mather. (2016). High-penetration PV integration handbook for distribution engineers. Technical Report of NREL. [Online]. Available: https://www.nrel.gov /docs/fy16osti/63114.pdf.

[34] J. Z. Zhu, "Optimal reconfiguration of electrical distribution network using the refined genetic algorithm", *Elect. Power Syst. Res.*, vol. 62, pp. 37-42, 2002.

[35] UNESP-FEIS Electrical Energy Systems Planning Laboratory Homepage, Test Systems. [Online]. Available: http://www.dee.feis.unesp.br/lapsee/.

[36] A. Halu, A. Scala, A. Khiyami, and M. C. González, Data-driven modeling of solar-powered urban microgrids, *Science Advances*, vol. 2, no. 1, pp. 1-9, Jan. 2016.

[37] A. Zare, C. Y. Chung, J. Zhan, and S. O. Faried, "A distributionally robust chance-constrained MILP model for multistage distribution system planning with uncertain renewables and loads," *IEEE Trans. Power Systems*, vol. 33, no. 5, pp. 5248-5262, Sept. 2018.

[38] J. Zhan, C. Y. Chung, and A. Zare, "A fast solution method for stochastic transmission expansion planning," *IEEE Trans. Power Syst.*, vol. 32, no. 6, pp. 4684–4695, Nov. 2017.

Junpeng Zhan (M'16) received B.Eng. and Ph.D. degrees in electrical engineering from Zhejiang University, China in 2009 and 2014, respectively.

He is currently a Research Associate Electrical Engineer at the Sustainable Energy Technologies Department, Brookhaven National Laboratory. He was a Postdoctoral Fellow in the Department of Electrical and Computer Engineering, University of Saskatchewan, Saskatoon, SK, Canada.

Weijia Liu received B.Eng. and Ph.D. degrees in electrical engineering from Zhejiang University, China in 2010 and 2015, respectively.

He is currently an Electrical Engineer at the National Renewable Energy Laboratory (NREL). He was a Postdoctoral Fellow in the Department of Electrical and Computer Engineering, University of Saskatchewan, Saskatoon, SK, Canada.

C. Y. Chung (M'01-SM'07-F'16) received B.Eng. (with First Class Honors) and Ph.D. degrees in electrical engineering from The Hong Kong Polytechnic University, Hong Kong, China, in 1995 and 1999, respectively.

He has worked for Powertech Labs, Inc., Surrey, BC, Canada; the University of Alberta, Edmonton, AB, Canada; and The Hong Kong Polytechnic University, China. He is currently a Professor, the NSERC/SaskPower (Senior) Industrial Research Chair in Smart Grid Technologies, and the SaskPower Chair in Power Systems Engineering in the Department of Electrical and Computer En-

gineering at the University of Saskatchewan, Saskatoon, SK, Canada. His research interests include smart grid technologies, renewable energy, power system stability/control, planning and operation, and power markets.

Dr. Chung is an Editor of *IEEE Transactions on Power Systems*, *IEEE Transactions on Sustainable Energy*, and *IEEE Power Engineering Letters* and an Associate Editor of *IET Generation, Transmission, and Distribution*. He is also an IEEE PES Distinguished Lecturer and a Member-at-Large (Global Outreach) of the IEEE PES Governing Board.

Jiajia Yang (STM'15-M'18) received his B.E. degree from Northeast Electric Power University, China, M.E. degree from Zhejiang University, China, and Ph.D. degree from the University of New South Wales, Australia, in 2011, 2014 and 2018 respectively, all in electrical engineering. He is currently a Research Associate in electrical engineering at the University of New South Wales, Australia. His research interests include electricity retailing, data mining in smart grid, renewable energy integration, and power markets.